Journal of Superconductivity, Vol. 12 No. 6, 1999, pp. 757-766.

# The Josephson effect in nanoscale tunnel junctions

**P. Joyez, D. Vion, M. Götz*, M. Devoret and D. Esteve**

*Service de Physique de l'Etat Condensé*
*CEA-Saclay, France*
**present address: PTB Braunschweig, Germany*

In nanoscale Josephson junctions, the Josephson coupling energy is usually comparable with the charging energy of the junction and with the typical energy of thermal fluctuations. Under these circumstances, phase fluctuations imposed by the electromagnetic environment of the junction crucially affect the junction electrical behavior. In particular they determine the maximum "supercurrent" the junction can sustain. We discuss this quantity in the case where the junction is not resistively shunted, so that the I-V characteristics of the junction remains hysteretic. For a simple, yet realistic unshunted junction model, we obtain detailed predictions of the shape of the supercurrent branch of the I-V characteristic. Finally we present experimental results supporting the theoretical analysis and which demonstrate that the supercurrent in an unshunted nanoscale Josephson junction can indeed be of the order of its critical current.

Key Words: Josephson effect, supercurrent, phase diffusion, switching current, escape rate

Running title: The Josephson effect in nanoscale tunnel junctions

## 1. Introduction

The prediction in 1962 of the Josephson effect [1] — and its observation soon afterwards — surprised the specialists of superconductivity at that time. It was found that a supercurrent of unexpectedly large magnitude can flow between two superconductors separated by an insulating tunnel barrier. The Josephson effect is a macroscopic quantum phenomenon: the supercurrent results from the coherent tunneling of Cooper pairs driven by the phase difference $\delta$ between the condensates of the two superconductors. Unlike the phase difference that can exist between two positions of a single particle wavefunction, $\delta$ is a collective variable directly coupled to macroscopic electric quantities in the circuit to which the junction is connected. Josephson showed that

$$\begin{aligned} \varphi_0 \frac{d\delta}{dt} &= v \\ i &= I_0 \sin\delta \end{aligned} \tag{1}$$

where $v$ and $i$ are the voltage and current operators for the junction, $I_0$ is the so-called critical current of the junction and $\varphi_0 = \hbar/2e$ the reduced flux quantum.

In large tunnel junctions like those studied immediately after the discovery of the effect, the phase

difference behaves as a classical quantity with little thermal fluctuations. The reason is that relatively large capacitance of the junction, tends to make the instantaneous voltage $v$ small and thus tends to suppress both thermal and quantum fluctuations of $\delta$.

However, in recent years, it has been possible with the advent of electron beam nanolithography to make junctions with area – and hence capacitance – so small that the fluctuations of $\delta$ are no longer determined almost essentially by the junction itself but by the circuit in which it is embedded, *i.e.* its electromagnetic environment. This can be apprehended by calculating the the r.m.s. amplitude of phase fluctuations in an approximation that replaces $\sin\delta$ by $\delta$ in (1): For small phase amplitude around $\delta = 0 \bmod 2\pi$ the junctions behaves as a linear inductor with inductance $L_0 = \varphi_0 / I_0$ and in this case, the r.m.s. amplitude of phase fluctuations are given by [2]

$$\sqrt{\langle \delta^2 \rangle} = \left( \int_{-\infty}^{+\infty} \frac{\mathrm{Re}\, Z_t(\omega)}{R_Q} \, \frac{1}{1 + e^{-\frac{\hbar\omega}{k_B T}}} \, \frac{\mathrm{d}\,\omega}{\omega} \right)^{1/2} \tag{2}$$

where $R_Q$ is the resistance quantum $h/4e^2 \simeq 6.5\,\mathrm{k}\Omega$, $k_B$ the Boltzmann constant, $T$ the temperature, and $Z_t$ is the total effective impedance of the inductance $L_0$ in parallel with the capacitance of the junction and with the impedance of the external circuit connected accross the junction. If the junction is small, its capacitance and effective inductance have high impedance on a broad frequency range over which $Z_t$ is entirely determined by the external circuit connected to the junction. One sees that depending on the circuit parameters, the fluctuations of $\delta$ can be large (*i.e.* comparable or larger than $2\pi$), in which case the instantaneous value of the supercurrent $I = \langle i \rangle = I_0 \langle \sin\delta \rangle$ flowing through the junction is washed out, even at $T = 0$. In order for the instantaneous supercurrent in a small Josephson junction to reach $I_0$ it is necessary to have small quantum spreading of the phase. This classical phase behavior requires that the total impedance is a broad-band low impedance ($Z_t \ll R_Q$). It turns out that this requirement is easily met, since ordinary leads connected to a junction are similar to transmission lines and present an impedance of the order of the vacuum impedance $Z_0 \simeq 377\,\Omega$. In fact, having quantum phase fluctuations survive in a small junction requires an engineering effort on the environment of the junction; it can be achieved for instance by microfabricating resistances in the junction leads, close to the junction [3].

As we have just explained, although a classical phase is a necessary condition to have a large supercurrent, it is however not sufficient to observe a large *static* supercurrent: the supercurrent may still classically time-average to nearly zero due to phase diffusion. The simplest way to limit phase diffusion is to shunt the junction on-chip with a low value resistance, and it indeed enables to reach static supercurrents of order $I_0$. However, this solution has a number of drawbacks when measuring the I-V characteristic of the junction :

i) the current flowing through the junction and the resistor cannot be measured independently, making it difficult to determine precisely the junction parameters. For instance, the verification of the quality of a tunnel junction by the measurement of the subgap quasiparticle current cannot be performed.

ii) the voltage scale of the characteristic is small; it is imposed by the resistor, not by the superconducting gap. Measuring it requires a very sensitive voltmeter.

iii) the characteristic is non-hysteretic; the shunted junction behaves as a mere non-linear resistor.

On the contrary, the switching behavior of an hysteretic junction provides an easy way to measure the maximum supercurrent.
The purpose of this article is to show that by engineering the electromagnetic environment of a small junction as a high-pass filter, one can indeed obtain supercurrents of the order of $I_0$ while the junction remains hysteretic. For a simple environment, we calculate analytically the switching current histograms. Finally, we present experimental results which support the theoretical analysis.

## 2. Theoretical analysis

### 2.1 Description of a tunnel junction coupled to its electromagnetic environment

Let us begin first describe the circuit we consider and see how, as we make the size of a tunnel junction smaller and smaller, Josephson phenomena depend on the environment of the junction. We take here for simplicity the basic case of an I-V measurement on a single junction. In such an experiment, the junction is biased with a dc current source $I_b$ through a series of filters. These filters are an essential part of the experiment: they ensure that the current fluctuations seen by the junction are well characterized thermal equilibrium fluctuations governed by a known temperature $T$ and not uncontrolled external noise. Likewise, the time-averaged voltage $V$ across the junction is measured through a similar series of filters. A schematic of the experimental set-up is shown in Fig. 1a where the linear quadrupoles $Q_I$ and $Q_V$ represent the filters and leads between the junction at low temperature and the current source and voltmeter at high temperature. The junction itself is described as a capacitance $C$ in parallel with a pure tunnel element characterized by the critical current $I_0$. At this stage, the critical current – not to be confused with the experimentally determined switching current – is just a measure of the Josephson coupling energy $E_J = \varphi_0 I_0$ which, for a junction with tunnel conductance $G_t$ separating two BCS superconductors with the same gap $\Delta$ , is given by $E_J = \frac{G_t R_Q}{2} \Delta$ [4]. Using Norton's theorem, the circuit viewed from the pure tunnel element can be replaced by a current source $I_b$ in parallel with a capacitance $C_0$, an admittance $Y(\omega)$ such that $\lim_{\omega \to 0} \frac{Y(\omega)}{\omega} = 0$ and a noise current source $i_n(t)$ (see Fig. 1b). We suppose furthermore that the filters are sufficiently well thermalized that the correlation function of the noise obeys the fluctuation-dissipation theorem [2]

$$\langle i_n(0)\, i_n(t) \rangle = \frac{k_B T}{\pi} \int_{-\infty}^{+\infty} \mathrm{Re}\, Y(\omega) \cos\omega t \, \mathrm{d}\omega \qquad (3)$$

where $T$ is the temperature of the filter stage close to the junction. Thus, $C_0$, $Y(\omega)$ and $T$ describe all the properties of the junction electromagnetic environment. Note that for small junctions the capacitance $C_0$ is not necessarily equal to the junction capacitance $C$ and can incorporate some stray capacitive effect of the leads close to the junction. An energy scale related with this capacitance which is often introduced in the context of small junction is the charging energy $E_C = e^2 / 2 C_0$ of a single electron on the capacitance $C_0$. In the case of small junctions such as those fabricated using

electron beam lithography, the junction area is typically $(100\,\mathrm{nm})^2$, and the maximum critical current density less than few $\mathrm{kA/cm^2}$ so that typically $E_J \sim E_C \sim 1\,k_B\,\mathrm{K}$.

### 2.2 Behavior of the junction at the plasma frequency

The highest frequency in the dynamics of the junction coupled to its electromagnetic environment is the plasma frequency $\omega_0^Y$, given by the modulus of the largest pole of $[Y(\omega) + i\,C_0\,\omega - i/L_0\,\omega]^{-1}$, where $L_0 = \varphi_0 / I_0$ is the effective inductance of the junction for small phase amplitude around $\delta = 0 \bmod 2\pi$. For usual circuits, at high frequency, $Y(\omega)$ is real and thus it can be replaced by $1/R$. In this case, for small phase amplitude the circuit is equivalent to a LC resonator with resonance frequency

$$\omega_0^Y = \frac{1}{\sqrt{L_0\,C_0}} = \frac{1}{\hbar}\sqrt{E_J\,E_C}$$

and a quality factor $Q_0$

$$Q_0 = R\sqrt{\frac{C_0}{L_0}} = \frac{\pi R}{R_Q}\sqrt{\frac{E_J}{2\,E_C}}\,.$$

Since $E_J \propto A$ and $E_C \propto A^{-1}$ where $A$ is the junction area (everything otherwise kept constant), one notices that $\omega_0^Y$ is independent of the size of the junction whereas $Q_0$ decreases with the area of the junction. For typical junction parameters, $\omega_0^Y$ falls in the 10 GHz range. At this frequency, as already discussed, the electromagnetic environment provided by typical leads presents an impedance of the order of the vacuum impedance $Z_0 \simeq 377\,\Omega \ll R_Q$. Thus, in small junctions, typical electromagnetic environment yields not only $\langle\delta^2\rangle^{1/2} \ll 1$, but also $Q_0 \ll 1$, and we will assume that this is the case in the following. Note that in large junctions, due to the scaling of the parameters with area, one can have both a classical phase and $Q_0 \ll 1$.

### 2.3 Phase dynamics

We are now ready to write down the equation of evolution for the classical phase accross the junction. The application of Kirchhoff's law to the circuit of Fig. 1b gives

$$C_0\,\varphi_0\,\ddot{\delta} + \varphi_0 \int_0^{+\infty} \dot{\delta}(t-\tau)\,y(\tau)\,\mathrm{d}\tau + I_0 \sin\delta = I_b + i_n(t) \qquad (4)$$

where $y(t) = \int_{-\infty}^{+\infty} Y(\omega)\exp(\mathrm{j}\omega t)\,\mathrm{d}\omega$ is the inverse Fourier transform of $Y(\omega)$. The time evolution of $\delta$ is, as is well known, identical to that of the position of a particle of mass $C_0\,\varphi_0^2$ in the tilted washboard potential $\varphi_0(-I_b - I_0\cos\delta)$, submitted to a random force $\varphi_0\,i_n(t)$ and a retarded friction force described by the kernel $\varphi_0^2\,y(t)$.

In the case of small junctions, the high damping at plasma frequency makes the current flowing in $C_0$ negligible compared to that flowing in $Y(\omega)$ and the first term of (4) can be dropped. This shows indeed that the charging energy of the junction, although large, is irrelevant here because the

environment can charge the capacitance $C_0$ much faster than the Josephson current. Consequently, in small junctions, the only inertial effects in the phase dynamics are due to the retarded friction.

### 2.4 Simple unshunted junction model

Even with this simplification, Eq. (4) remains an integro-differential equation with noise, for which there is no general analytical method. In the following, we will consider for definiteness the simplest non-trivial case describing a realistic situtation and for which we are still able to obtain analytical results in some limits. Specifically, we take $Y(\omega)$ to be a resistor $R_0$ in parallel with a capacitor-resistor series combination characterized by the capacitance $C_1$ and resistance $R_1$ (see Fig. 1c).

$$Y(\omega) = R_0^{-1} + \frac{1}{R_1 + (j\,C_1\,\omega)^{-1}} \tag{5}$$

This model reduces to the resistively shunted junction (RSJ) model of Fig. 1d for $\omega \neq 0$ when $R_1\,C_1 \to \infty$ (RSJ limit) or and to the resistively and capacitively shunted junction (RCSJ) model [5, 6, 7] when $R_1 \to 0$. The resistance $R_0$ can describe an on-chip shunting resistor across the junction, but in the following we will rather think of it as the finite dc shunt resistance of the current bias and voltage measurement circuitry which, in actual experiments, can vary between a few kΩ and a few MΩ. The $R_1 - C_1$ combination describes the high frequency cut-off behavior of the filtering system. It is important to note that one can, as was done in the experiment reported below, build an on-chip filter that ensures that our 3-element model for $Y(\omega)$ given by Eq. (5) closely describes reality.

By introducing the voltage $u(t)$ across the capacitor $C_1$, one can show that for our model, Eq. (4) is equivalent to the set of two first order coupled differential equations

$$\varphi_0\,\dot{\delta} = R_{//}\Big(I_b + i_{0\,n} + \tfrac{u}{R_1} + i_{1\,n} - I_0 \sin\delta\Big) \tag{6}$$

$$R_1\,C_1\,\dot{u} = R_{//}\Big(I_b + i_{0\,n} - \frac{R_1}{R_0}\,i_{1\,n} - I_0 \sin\delta - \frac{u}{R_0}\Big) \tag{7}$$

In the last two equations $R_{//} = \frac{R_0\,R_1}{R_0 + R_1}$ and the noise sources $i_{0\,n}(t)$ and $i_{1\,n}(t)$ in parallel with the resistances $R_0$ and $R_1$ verify

$$\langle i_{j\,n}(t)\,i_{j\,n}(t)\rangle = \frac{2\,k_B\,T}{R_j}\,\delta(t) \qquad j = 0,\,1$$

where $\delta(t)$ is here the Dirac delta function, not the phase difference. This analysis shows that the phase space of the model of Fig. 1c has two dimensions. More generally, if $Y(\omega)$ has $N$ poles, the integro-differential Eq. (4) is equivalent to $N + 1$ first order coupled differential equations (the capacitance $C_0$, if kept, adds another differential equation and can be thought of as contributing to the total admittance seen by the junction by a pole at $\omega = \infty$ ).

### 2.5 Solving the dynamics: adiabatic approximation

Unfortunately, even within our restricted model of admittance, there is still no general method to solve Eqs. (6) and (7) with the noise terms, and in the most general case, one has to resort to numerical simulation. However, from the analysis of the deterministic behavior of the system at zero temperature [7, 8, 9], one sees that a fluctuation resilient supercurrent reaching $I_0$ can only be achieved in the RSJ limit, which therefore is the optimum case. Concretely, this means that the dynamics of $\delta$ must be overdamped at all frequencies. In the case of an unshunted junction, this is done by slowing down the dynamics of $u$ as much as possible. It turns out that in this limit, the effect of thermal fluctuations on the behavior of the system is amenable to detailed predictions which we now explain.

From Eqs. (6) and (7) one sees that the characteristic evolution time for $\delta$ is $\varphi_0 / R_{//} I_0$ and that of $u / R_{//} I_0$ is $R_1 C_1$. By choosing the parameters of the environment such that the damping parameter $\alpha = R_1 R_{//} C_1 I_0 / \varphi_0 \gg 1$, one can make the time evolution of $u / R_{//} I_0$ much slower than that of $\delta$. This can safely be achieved by taking large enough $C_1$, whereas increasing the resistances will ultimately result in the violation of the hypothesis of high damping at the plasma frequency and of classical phase behavior. If this decoupling of timescales condition is met ($\alpha \gg 1$), one can then use an adiabatic approximation for $u$: First, one solves (6) with $u$ taken as a constant parameter and then, using this solution, one can solve (7) for the slow $u$ dynamics. The first step is easy since the system is then equivalent to that of the RSJ model with a current source $I_b'(u) = I_b + u / R_1$ and a shunt resistor $R_{//}$, for which many analytical results are known (see [10] and appendix A). In particular, the average current flowing through the junction is given by

$$I(u) = I_0 \langle \sin \delta \rangle_u = I_0 \, \mathrm{Im}\left[ \frac{I_{1-i\eta(\frac{E_J}{k_B T})}}{I_{-i\eta(\frac{E_J}{k_B T})}} \right] \tag{8}$$

with

$$\eta = \frac{I_b'(u) E_J}{I_0 k_B T}$$

and the average voltage drop across the junction is given by

$$V(u) = R_{//}(I_b'(u) - I(u)). \tag{9}$$

We thus obtain a parametrically defined temperature-dependent I-V characteristic which is plotted in Fig. 2.

### 2.6 Slow dynamics: the switching process

Using this adiabatic solution and (7), one can determine the static solutions for $u$. These solutions may be obtained graphically , as shown in Fig. 3, by contructing the intersection between the load line of the true source $I_b \,//\, R_0$ source and the I-V characteristic of the junction parametrically determined by Eq. (8) and (9). If $1/R_0$ is larger than the maximum of the absolute value of the negative differential conductance of the junction, then there is only one solution for $u$ which is obviously stable (point $\mathcal{S}$ in Fig. 3a). On the other hand, in a current bias mode, *i.e.* $R_0 \to \infty$, one is more likely to be in a situation depicted in Fig. 3b where there are three static solutions for $u$. This corresponds to the usual hysteretic behavior of unshunted Josephson junctions: The high voltage state corresponds to the "running state" of the phase, and usually sits on the quasiparticle current branch of the characteristic of the junction (point $\mathcal{S}$ in Fig. 3b). This running state is stable. The solution at intermediate voltage (point $\mathcal{U}$) is an unstable solution and cannot be observed in practice in this bias mode. The lowest voltage solution (point $\mathcal{M}$) corresponds to the "phase diffusion state" which is the remnant of the true superconducting state of large Josephson junctions. In this state, the phase has a low average velocity; it spends most of its time trapped in the wells of the tilted washboard. However, this state is only metastable: if some fluctuations cause an increase of the phase velocity beyond that corresponding to the velocity of the unstable solution, then the junction switches to the running state. This switching process is not of the usual "escape over a potential barrier" class, since the system switches between two dissipative dynamical states. However, the present problem can be mapped onto a problem of the usual class, as we now explain.

The equation for the slow evolution of $u$ is given by (7). We replace $\sin\delta$ by $\langle \sin\delta \rangle_u + \eta_u(t)$ corresponding to the average values plus fluctuations around this average, so that (7) can be rewritten as the Langevin-like equation:

$$\left(1 + \frac{R_1}{R_0}\right) C_1 \, \dot{u} = I_b - I_0 \, \langle \sin\delta \rangle_u - \frac{u}{R_0} - I_0 \, \eta_u(t) + i_{0\,n}(t) - \frac{R_1}{R_0} \, i_{1\,n}(t) \tag{10}$$

which corresponds to the equation of motion of a massless particule at position $u$, submitted to a deterministic force $F(u) = I_b - I_0 \, \langle \sin\delta \rangle_u - \frac{u}{R_0}$, a viscous damping force $-\lambda \, \dot{u} = -\left(1 + \frac{R_1}{R_0}\right) C_1 \, \dot{u}$, and a position dependent random force $\xi(t) = -I_0 \, \eta_u(t) + i_{0\,n}(t) - \frac{R_1}{R_0} \, i_{1\,n}(t)$. Note that $\eta_u(t)$ is rigorously a coloured noise term, but here, owing to the decoupling of timescales, it can be treated as $\delta$-correlated.

One can thus use a generalization of Kramers' large friction result with position-dependent diffusion constant (see appendix B) to evaluate the escape rate of $u$ over the effective potential barrier given by $-\int F(u) \, \mathrm{d}\, u$ . The result takes an Arrhenius-like form:

$$\Gamma = \frac{D(u_t)}{2\pi} \sqrt{\left(\frac{-F}{\lambda D}\right)'_{u_b} \left(\frac{F}{\lambda D}\right)'_{u_t}} \, \exp(B) \tag{11}$$

where $D = \frac{1}{\lambda^2} \int_0^{+\infty} \xi(0) \, \xi(t) \, d\, t$ is the diffusion coefficient associated with the random force which can be calculated with the use of (19) and (22), $B = \int_{u_b}^{u_t} \frac{F}{\lambda D} \, \mathrm{d}\, u$, and $u_b$ and $u_t$ stand, respectively,

for the bottom and the top of the effective potential barrier. The main result of our calculation is that $B \propto \alpha$ which shows that indeed, for $I_b < \underset{u}{\mathrm{Max}}\left( I_0 \langle \sin\delta \rangle_u + \frac{u}{R_0} \right)$, the switching rate can be made as low as desired by increasing the damping on $u$. This can be simply interpreted saying that as the $R_1 C_1$ circuit integrates fluctuations for a longer time, the premature switching of the junction due to fluctuations diminishes.

## 3. Experiments

### 3.1 Sample description

Our experiment tests the predictions of Eqs. (8) and (9) for the voltage in the diffusion state and of Eq. (11) for the switching rate. It is performed on a sample consisting of two circuits implementing Fig. 4a. Even though the schematics of our experimental circuit differs from our model circuit (Fig 1c), Norton's theorem shows that they are electrically equivalent (Fig. 4b). The sample fabrication involved four steps. First, a gold ground plane forming one plate of the capacitors $C_1$ was deposited on a Si wafer and covered by a silicon nitride insulating layer. Then two different resistors $R_1$ were made by optical lithography and evaporation of an AuCu alloy. The other plates of the $C_1$ capacitors and the junction pads involved another optical lithography step and evaporation of pure Au. Finally, two nominally identical Al-AlOx-Al Josephson junctions were fabricated using *e*-beam lithography and double angle shadow mask evaporation [11]. We estimate the capacitances $C_0 = 8 \pm 2$ fF of the junctions from their area. The capacitance $C_1 = 150$ pF was measured at room temperature. The sample was mounted in a copper box thermally anchored to the mixing chamber of a dilution refrigerator. The electrical wiring for the bias and voltage leads was made using coaxial lines with miniature cryogenic filters [12]. The resistances $R_1$ and the superconducting energy gap of the junctions were measured on the I-V characteristics at 30 mK in zero magnetic field. The junction critical currents were obtained from the Ambegaokar-Baratoff relation [4] using the measured tunnel resistances in the normal state. The parameters characterizing the two circuits referred to in the following as #1 and #2 were $I_0 = 40.1$ nA, $R_1 = 70\,\Omega$, $Q_0 \simeq 0.079$, $\alpha = 83$ and $I_0 = 37.5$ nA, $R_1 = 540\ \Omega$, $Q_0 \simeq 0.58$, $\alpha = 5100$, respectively. In our setup, the resitance $R_0 = 35\,\mathrm{k}\Omega$ of the current source was much larger than $R_1$ and was considered as infinite in the data analysis. The bias current was ramped at constant speed $dI_b/dt$.

### 3.2 Supercurrent branch

We show in Fig. 5 a typical I-V characteristic, obtained for circuit #1 at 40 mK. The branch corresponding to the diffusion state appears vertical on this large scale. It is interrupted at the switching current $I_S$ which fluctuates from one ramp cycle to another. A histogram of $I_S$ is shown in the inset. In Fig. 6 we show diffusion branches measured using a lock-in technique for both circuits and for different temperatures. At a given current bias, the voltage across the junction, which measures phase diffusion, increases with temperature and is larger for circuit #2 than for circuit #1. We also show in Fig. 6 the curves $I(V) = I_0 \langle \sin \delta \rangle_u + I_{QP}(V)$ where $u = V - R_1 I_0 \langle \sin \delta \rangle_u$, predicted by our model using the measured parameters. The correction $I_{QP}(V)$ due to quasiparticles was calculated using BCS theory [13]. Its relative importance attains only 20% for the highest temperature. The agreement between experimental and calculated curves is quantitative for circuit #1 and only qualitative for circuit #2. By varying $I_0$ with a small magnetic field, we checked that the discrepancy at low temperature between theory and experiment for circuit #2 could not be explained by some remaining external noise on the sample or Joule heating in the resistor. We attribute the discrepancy to the fact that circuit #1 fully satisfies the hypotheses of our calculation ($Q_0 \ll 1$ and $\alpha \gg 1$) while for circuit #2, $Q_0 \simeq 0.58$. However, agreement is recovered at high temperature by performing numerical simulations including $C_0$ (data not shown). At low temperature, quantum fluctuations of the phase lower the $\langle \sin \delta \rangle_u$ curves [14] and could be taken into account to make a more accurate theoretical prediction [15]. Note that even when $\delta$ can fluctuate quantum mechanically because $Q_0$ is not small enough, $u$ remains a classical variable and the switching is an entirely classical process.

### 3.3 Switching current

Histograms of the current $I_S$ obtained from 8000 switching events were measured as a function of temperature in order to test the predictions of Eq. (11). The measured histograms were first converted into ln $\Gamma(I_b)$ sets of data points by the method of Fulton and Dunkleberger [16]. For a given temperature, these data points fall on a single curve independent of $dI_b/dt$ (data not shown). It is convenient to characterize the current dependence of the rate at a given temperature by two values: the average switching current $\langle I_S \rangle$ and the standard deviation $\Delta I_S$. These values are shown in Fig. 7 together with theoretical predictions. The averages $\langle I_S \rangle / I_0$, which decrease with temperature, are nearly identical for both circuits. However, $\Delta I_S$ is about 1 order of magnitude higher for circuit #1 than for circuit #2. Furthermore, $\Delta I_S$ for circuit #1 decreases significantly when $k_B T > 0.2 E_J$. These effects are well explained by our calculation. At a given temperature, the exponent $B$ vanishes when $I_b$ reaches the maximum of the $I_0 \langle \sin \delta \rangle_u$ curve. Thus, in the limit $\alpha \to \infty$, $\langle I_S \rangle / I_0 = \mathrm{Max}(\langle \sin \delta \rangle_u)$ [dashed line in Fig. 7a]. As damping is decreased, the dissipation barrier height decreases ($B \propto \alpha$), and thermal fluctuations driving $u$ above the dissipation barrier induce premature switching. The predicted curve $\langle I_S \rangle / I_0$ for circuit #1 [solid line in Fig. 7a] shows this effect and fits the experimental data. The corresponding curve for circuit #2 is indistinguishable from the $\mathrm{Max}(\langle \sin \delta \rangle_u)$ and agrees only qualitatively with the data. We attribute this discrepancy to the aforementioned large value of $Q_0$. The large increase in the width of the histogram when going from circuit #2 to circuit #1 is a more direct manifestation of the effect of damping [see Fig. 7b]. As the damping $\alpha$ decreases, the relative change in the barrier height with $I_b / I_0$ and, consequently, the slope of $\Gamma(I_b)$ decreases. Finally, the decrease of $\Delta I_S$ at high temperature is a consequence of the rounding of $\langle \sin \delta \rangle_u$ with increasing $k_B T / E_J$.

## 4. Conclusion

To summarize, a small unshunted current-biased junction connected to a RC impedance switches from a phase diffusion branch to a voltage branch by a process entirely different from the switching in large area junctions. This process is not dominated by thermal activation over the usual washboard potential barrier (or quantum tunneling through this barrier) but by thermal activation above a dissipation barrier for which an expression can be found in the large friction limit. The predictions based on this expression are well verified experimentally. When R increases, the width of switching histograms decreases, a direct consequence of the scaling of the dissipation barrier with the RC time constant of the impedance. The effect of temperature is twofold. It modifies the dependence of the dissipation barrier on bias current as well as producing the fluctuations driving the system above this barrier. This complexity must be taken into account if the average value of the switching current is to be used as a measurement of the critical current. Finally, the current dependence of the voltage in the diffusion state prior to switching is directly related to the shape of the dissipation barrier. Our results indicate that the dissipation barrier can be affected by quantum fluctuations of the phase difference when $Q_0$ is not small enough. Precise measurements of the voltage prior to switching as a function of $Q_0$ in the large $\alpha$ regime would improve our knowledge of the quantum diffusion process in the tilted washboard.

## Acknoledgements

We are indebted to M. Goffman, H. Grabert, R. Kautz, J. Martinis and C. Urbina for useful discussions. This work has been partly supported by the Bureau National de la Métrologie and the European project SETTRON.

**Note added in proof:**
Since this article was written, new predictions concerning the reduction of the supercurrent due to quantum phase fluctuations have become available [H. Grabert, G.-L. Ingold and B. Paul, Europhys. Lett. **44**, 360-366 (1998), and G.-L. Ingold and H. Grabert, cond-mat archive 9904256]. These predictions are consistent with the low temperature saturation of the switching current we observe for circuit #2.

## Appendix A: average current and current fluctuations in the RSJ model

In this appendix, we give the details of the calculation of the average current $I_0 \langle \sin \delta \rangle$ and of the zero-frequency spectral density $d = \int_0^\infty [\langle \sin\delta(\tau) \sin\delta(0) \rangle - \langle \sin\delta \rangle^2] \, \mathrm{d}\tau$ for a heavily damped junction. Our derivation closely follows that of Ivanchenko and Zil'berman who first derived the I-V characteristic of a junction in the RSJ model [17]. Their starting point is the equation of evolution for the phase in the circuit depicted in Fig. 8.

$$\varphi_0 \frac{d\delta}{dt} + R I_0 \sin\delta = V + e(t) \tag{12}$$

where $e$ is the fluctuating emf generated by the resistor which satisfies $\langle e(0)\, e(t)\rangle = 2 k_B T R \delta(t)$. Introducing the reduced variables $\tau = R I_0 t/\varphi_0$, $\epsilon = e/R I_0$, $u = V/R I_0$, and $\Theta = k_B T/E_J$, (12) rewrites as

$$\frac{d\delta}{d\tau} + \sin\delta = v + \epsilon(\tau) \tag{13}$$

with $\langle \epsilon(0)\, \epsilon(t)\rangle = 2\Theta\delta(\tau)$. Then, they introduce the density of probability $W(\delta, \tau \mid \delta_0, \tau_0)$ of having the phase $\delta$ at time $\tau$ when it was $\delta_0$ at $\tau_0$, and its Fourier series $x_n(\tau) = \int_{-\infty}^{+\infty} e^{i n \delta} W(\delta, \tau \mid \delta_0, 0)\, d\delta$, which obey the Fokker-Planck equations equivalent to (13):

$$\frac{dW}{d\tau} = \frac{d^2 W}{d\delta^2}\Theta + W\cos\delta + \frac{dW}{d\delta}(\sin\delta - u) \tag{14}$$

$$\frac{dx_n}{d\tau} = -n\left[(\Theta n - i u)\, x_n + \frac{x_{n+1} - x_{n-1}}{2}\right] \tag{15}$$

In the limit $\tau \to \infty$, the system reaches a steady-state described by $W_\infty(\delta) = W(\delta, \infty \mid \delta_0, \tau_0)$ independently the initial state $\delta_0$ and $\tau_0$. One then sees that $x_n(\infty)$ obeys an homogeneous difference-recurrence relation

$$2(\Theta n - i u)\, x_n(\infty) = x_{n-1}(\infty) - x_{n-1}(\infty) \tag{16}$$

which can be solved numerically or in terms of continued fractions [10, 18]. Instead of this, Ivanchenko and Zil'berman noticed the similarity with the recurrence relation obeyed by Bessel functions

$$2\eta I_\eta(z) = z(I_{\eta-1}(z) - I_{\eta+1}(z)) \tag{17}$$

which leads to a compact analytical result. Identifying (16) and (17) and using the fact that $W$ is real and normalized, which imposes the constraints that $x_n = x_{-n}^*$ and $x_0 = 1$, one has the unique solution

$$x_{|n|}(\infty) = \frac{I_{|n| - i u/\Theta}(1/\Theta)}{I_{-i u/\Theta}(1/\Theta)}$$

This result yields the average current flowing through the junction

$$I = I_0 \langle \sin\delta\rangle = I_0\left(\frac{x_1(\infty) - x_{-1}(\infty)}{2i}\right) = I_0 \operatorname{Im}[x_1(\infty)] \tag{18}$$

To go further, we need to know about the fluctuations of the current around this mean value. In fact, as shown in sec. 2.6, for the purpose of evaluating the switching current it is enough to calculate the zero-frequency spectral density of $\sin\delta$

$$d = \int_0^\infty [\langle \sin\delta(\tau)\sin\delta(0)\rangle - \langle\sin\delta\rangle^2]\, d\tau \tag{19}$$

To proceed, we introduce the quantities

$$s_n = \int_0^\infty (\langle e^{i n \delta(\tau)} \sin\delta(0)\rangle - \langle e^{i n\delta}\rangle \langle \sin\delta\rangle)\, d\tau$$

$$= \int_0^\infty d\tau \int_{-\infty}^{+\infty} d\delta_0 \int_{-\infty}^{+\infty} d\delta\, e^{i n\delta} \sin\delta_0\, W_\infty(\delta_0)\, \{W(\delta, \tau \mid \delta_0, 0) - W_\infty(\delta)\} \tag{20}$$

which verify $s_0 = 0,\ s_n = s_{-n}^*$, and $d = \mathrm{Im}[s_1]$. Upon integration by part of (20) over $\tau$ and using (18) one obtains the relation

$$(n\,\Theta - i\,u)\,s_n + \tfrac{s_{n+1}-s_{n-1}}{2} = x_n(\infty) \quad [i\,\Theta + \tfrac{u-\mathrm{Im}[x_1(\infty)]}{n}] \tag{21}$$

Finally, $s_1$ is obtained by eliminating the $s_n$, $n > 1$ by summing all equations (21) with proper multiplicative factor. Working out this elimination, it turns out that the multiplicators verify a difference-recurrence relation similar to (16) and whose solution is $(-1)^n\,x_n(\infty)$, so that

$$s_1 = -2\sum_{n=1}^{\infty}(-1)^n\,(x_n(\infty))^2[i\ \Theta + \tfrac{u-\mathrm{Im}[x_1(\infty)]}{n}].$$

Hence, the zero-frequency spectral density is obtained by a summing a rapidly converging series

$$d = -2\sum_{n=1}^{\infty}(-1)^n\,\mathrm{Im}\,\{(x_n(\infty))^2[i\ \Theta + \tfrac{u-\mathrm{Im}[x_1(\infty)]}{n}]\}. \tag{22}$$

## Appendix B: Kramers escape rate for position-dependent strong friction.

In this appendix, we generalize Kramers' strong friction result [19] to the case of a position-dependent diffusion constant, a result which is needed to evaluate the switching rate of small junctions. The starting point is the Langevin equation of a massless particle moving on the $x$ axis submitted to a systematic force $F(x)$, a viscous damping force $-\lambda\,\dot{x}$ and a position-dependent random force $\xi(x,\,t)$.

$$\lambda\,\dot{x} = F(x) + \xi(x,\,t).$$

The systematic force derives from a potential having a local minimum at $x_b$ and a local maximum at $x_t > x_b$. The particle being initially trapped at the local minimum, we want to estimate its escape rate under the influence of the random force. As usual in Kramer's approach, the escape rate is assumed to be small. In this case, the density of probability $\rho(x)$ of finding the particle at position $x$ can be approximated by a steady state density of probability obeying the relation

$$j = \rho(x)\,v(x) - D(x)\ \tfrac{d\,\rho}{d\,x},$$

where $j$ is the current, $v(x) = F(x)/\lambda$ the drift velocity and $D(x)=\int_0^{\infty}\langle\dot{x}(x,\,t)\,\dot{x}(x,\,0)\rangle\,\mathrm{d}\,t$ is the position-dependent diffusion constant. Note that in our problem the extra drift velocity $-D'(x)/2$ due to the spatial dependence of $D$ [18] is completely negligible and ommited here. Assuming an absorbing boundary condition at $x_+ \gg x_t$, the solution to this differential equation is of the form

$$\rho(x) = j\,\rho_0(x)\int_x^{x_+}\frac{\mathrm{d}\,x'}{D(x')\,\rho_0(x')}$$

where

$$\rho_0(x) = \exp\int_{x_b}^{x}\tfrac{F(\,x')}{\lambda\,D(x')}\ \mathrm{d}\,x'$$

would be the equilibrium solution. The escape rate is given by the ratio of the current to the total population

$$\Gamma = j \Big/ \int_{-\infty}^{x_+} \rho(x)\, d\, x = \left( \int_{-\infty}^{x_+} \mathrm{d}\, x\, \rho_0(x) \int_{x}^{x_+} \frac{\mathrm{d}\, x'}{D(x')\rho_0(x')} \right)^{-1}.$$

This integral can be evaluated using a Gaussian steepest-descent approximation for $\rho_0$ at $x = x_b$ and for $1/\rho_0$ at $x = x_t$ . This yields the sought result

$$\Gamma \simeq \frac{D(x_t)}{2\pi} \sqrt{\left(\frac{-F}{\lambda D}\right)'_{x_b} \left(\frac{F}{\lambda D}\right)'_{x_t}}\, \exp\left( \int_{x_b}^{x_t} \frac{F(x')}{\lambda D(x')}\, \mathrm{d}\, x' \right).$$

## References


[1] B. D. Josephson, in *Superconductivity*, R. D. Parks Ed. (M. Dekker, New York, 1969)

[2] G.-L. Ingold, in *Quantum processes and dissipation*, (Wiley-VCH, 1998).

[3] L. S. Kuzmin and D. B. Haviland, Phys. Rev. Lett. **67**, 2890 (1991).

[4] V. Ambegaokar and A. Baratoff, Phys. Rev. Lett. **10**, 486 (1963).

[5] W. C. Stewart, Appl. Phys. Lett. **12**, 277 (1968).

[6] D. E. McCumber, J. Appl. Phys. 39, 3113 (1968).

[7] R. L. Kautz and J. M. Martinis, Phys. Rev. **B 42**, 9903 (1990). J. M. Martinis and R. L. Kautz, Phys. Rev. Lett. 63, 1507 (1989).

[8] M. H. Devoret, P. Joyez, D. Vion and D. Esteve, in *Macroscopic Quantum Phenomena and Coherence in Superconducting Network*, C. Giovanella and M. Tinkham Eds., (World Scientific, Singapore, 1995).

[9] P. Joyez, PhD Thesis (university Paris VI, Paris, 1995).

[10] W. T. Coffey, Yu. P. Kalmykov and J. T. Waldron, *The Langevin Equation* (World Scientific, 1996)

[11] G. J. Dolan and J. H. Dunsmuir, Physica (Amsterdam) 152B, 7 (1988).

[12] D. Vion, P. F. Orfila, P. Joyez, D. Esteve, and M. H. Devoret, J. Appl. Phys. 77, 2519 (1995).

[13] A. Barone and G. Paternò, Physics and Applications of the Josephson Effect (Wiley, New York, 1992), p. 39.

[14] G. L. Ingold, H. Grabert, and U. Eberhardt, Phys. Rev. B 50, 395 (1994).

[15] H. Grabert and B. Paul (private communication).

[16] T. Fulton and L.N. Dunkleberger, Phys. Rev. B 9, 4760 (1974).

[17] Yu. M. Ivanchenko and L. A. Zil'berman, Zh. Eksp. Teor. Fiz. **55**, 2395 (1968) translated in Sov. Phys. JETP 28, 1272 (1969).

[18] H. Risken, *The Fokker-Planck Equation* (Springer-Verlag, Berlin, 1984)

[19] P. Hänggi, P. Talkner and M. Borkovec, Rev. Mod. Phys. **62**, 2 (1990)

## Figure Captions

FIG. 1. A Josephson junction with its measurement circuitry (a) can be modelled as a tunnel element (cross) in parallel with a capacitance, an electromagnetic environment admittance $Y(\omega)$, a bias current source and a noise current source (b). Circuit (c) shows the simple model of $Y(\omega)$ discussed in this paper. In the limit where $R_1 C_1 \to \infty$ and $C_0 = 0$ this circuit becomes equivalent to (d) for which many properties are known.

FIG. 2. I-V characteristics of a junction in the RSJ model of Fig 1d at different temperatures. Inset: Temperature dependence of the maximum of the I-V characteristic.

FIG. 3. Geometric construction yielding the voltage across the junction. In the case where $R_0$ is low (a), the bias source corresponds to a voltage source, and only one voltage is possible (point $\mathcal{S}$). We are more interested in the case where $R_0$ is high (b), which corresponds to a current source, there are three possible voltages: one is stable (point $\mathcal{S}$) and corresponds to the running state of the phase, the second ($\mathcal{U}$) is unstable and thus inobservable, the last ($\mathcal{M}$) sits on the phase diffusion branch and is only metastable.

FIG. 4. a) Schematics of the experimental circuit. Although this setup is different from our model environment of Fig. 1c, by use of Norton's theorem (b), they are indeed electrically equivalent but with different circuit parameters (here $\lambda = 1 + \frac{R_0}{R_1}$ and $u' = \lambda u - R_1 I_b$).

FIG. 5. Large scale I-V characteristic of a Josephson junction corresponding to the circuit of Fig. 2. The switching at current $I_S$ from the diffusion branch (vertical branch in the center of the characteristic) to the quasiparticle branch of the junction is a random process. Inset shows histogram of $I_S$ measured at $\mathrm{d}(I/I_0)/\mathrm{d}t = 8.5\ \mathrm{s}^{-1}$ for circuit #1.

FIG. 6. Experimental (solid lines) and theoretical (dotted lines) diffusion branches of two circuits of the type in Fig. 2. Top: circuit #1 at T - 47, 110, 330, 422, 598, 700, and 809 mK (from top to bottom). Experimental data corresponding to the two lowest temperature are barely distinguishable. Bottom: circuit #2 at T - 47, 100, 140, 193, 253, 312, 372, 448, 535, 627, 718, and 813 mK (from top to bottom).

FIG. 7. Experimental (dots) and theoretical (lines) switching current average $\langle I_S \rangle$ (a) and r.m.s. deviation $\Delta I_S$ (b) as a function of the dimensionless temperature $k_B T / E_J$ for circuits #1 and #2.

FIG. 8. Voltage biased junction with resistor. The noise due to fluctuation in the resistor is represented by the fluctuating voltage source $e(t)$. The $I(V)$ law of this circuit can be calculated analytically for arbitrary temperature, and thus gives access to the I-V charateristic of the junction itself. Note that in virtue of Norton's theorem, this circuit is equivalent to the RSJ circuit of Fig. 1d.

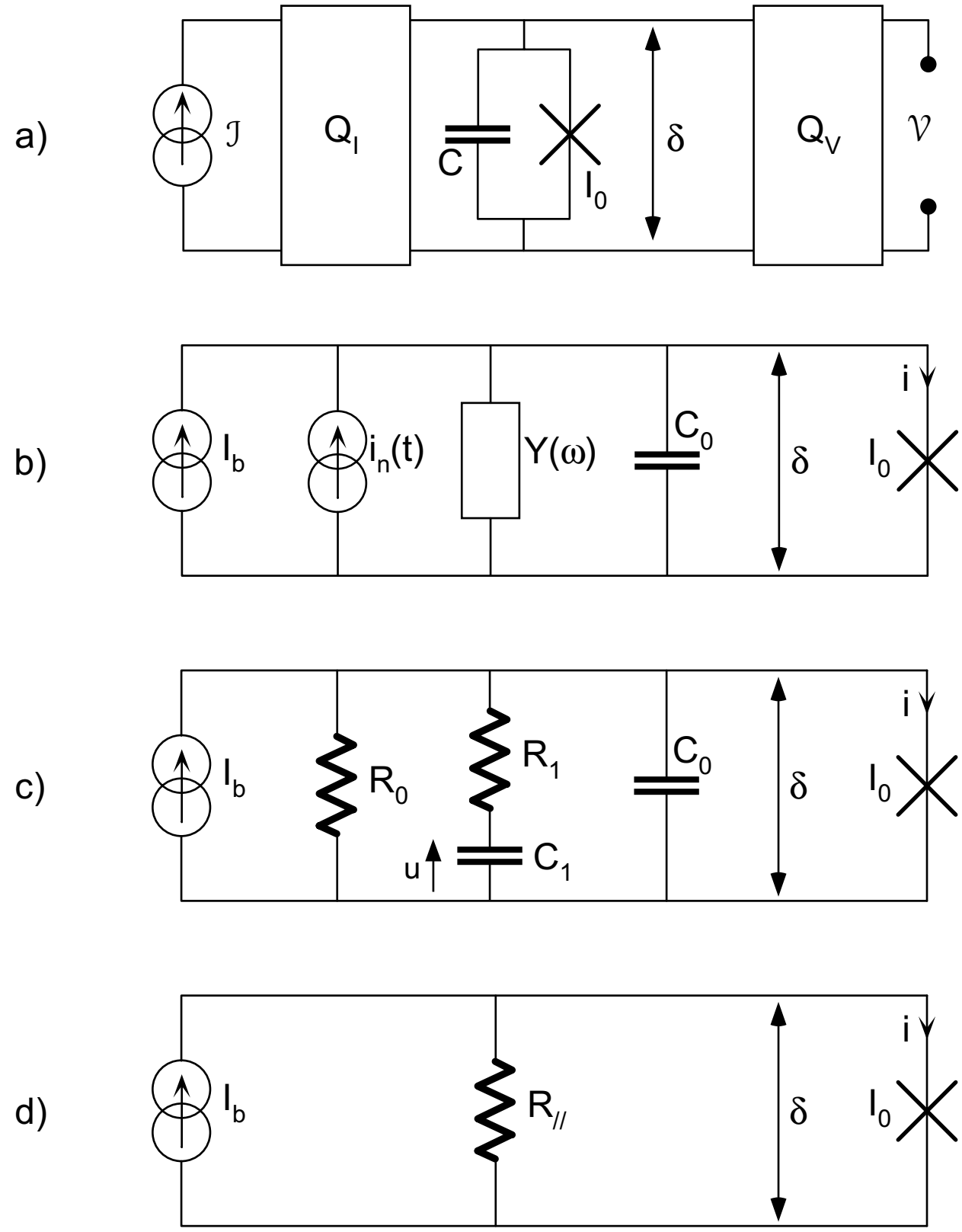
a)
$\mathcal{I}$
$Q_I$
C
$I_0$
δ
$Q_V$
$\mathcal{V}$
b)
$I_b$
$i_n(t)$
Y(ω)
$C_0$
δ
i
$I_0$
c)
$I_b$
$R_0$
$R_1$
u
$C_1$
$C_0$
δ
i
$I_0$
d)
$I_b$
$R_{//}$
δ
i
$I_0$

Fig. 1

# Fig. 2

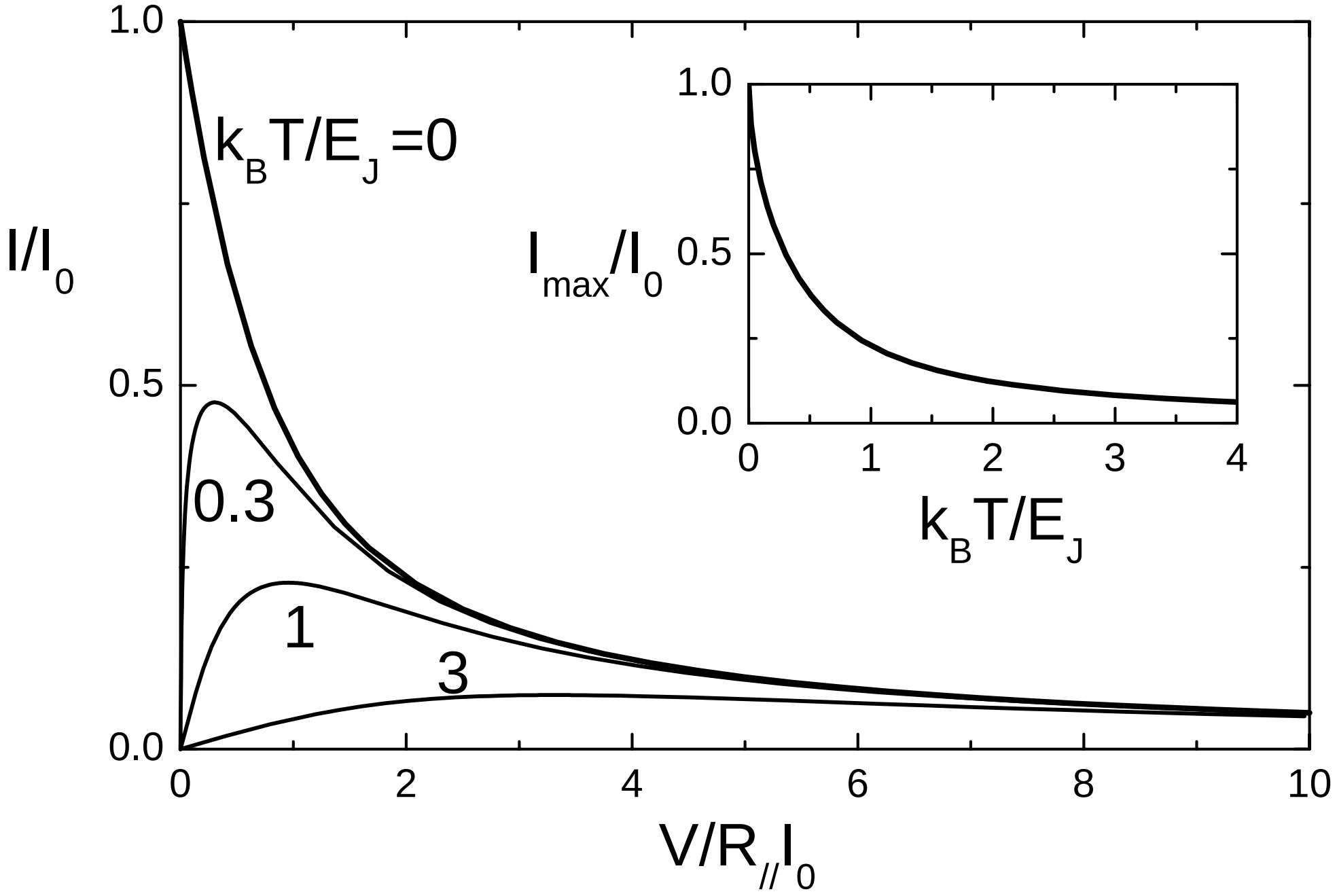
1.0
0.5
0.0
0
2
4
6
8
10
I/I0
V/R// I0
kBT/EJ =0
0.3
1
3
Imax/I0
1.0
0.5
0.0
0
1
2
3
4
kBT/EJ

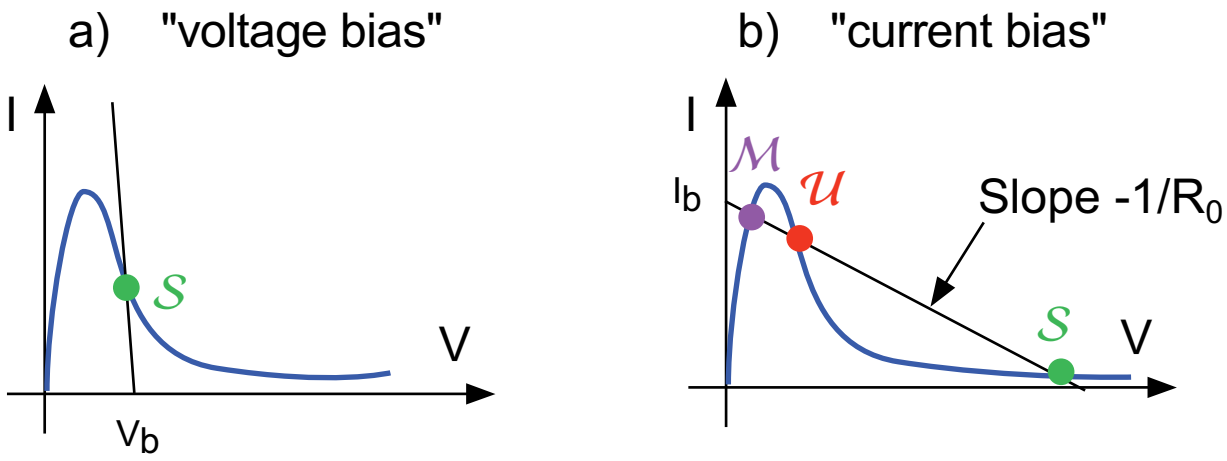
a) "voltage bias"
I
V
$\mathcal{S}$
$V_b$
b) "current bias"
I
$I_b$
$\mathcal{M}$
$\mathcal{U}$
Slope -1/$R_0$
$\mathcal{S}$
V

Fig. 3

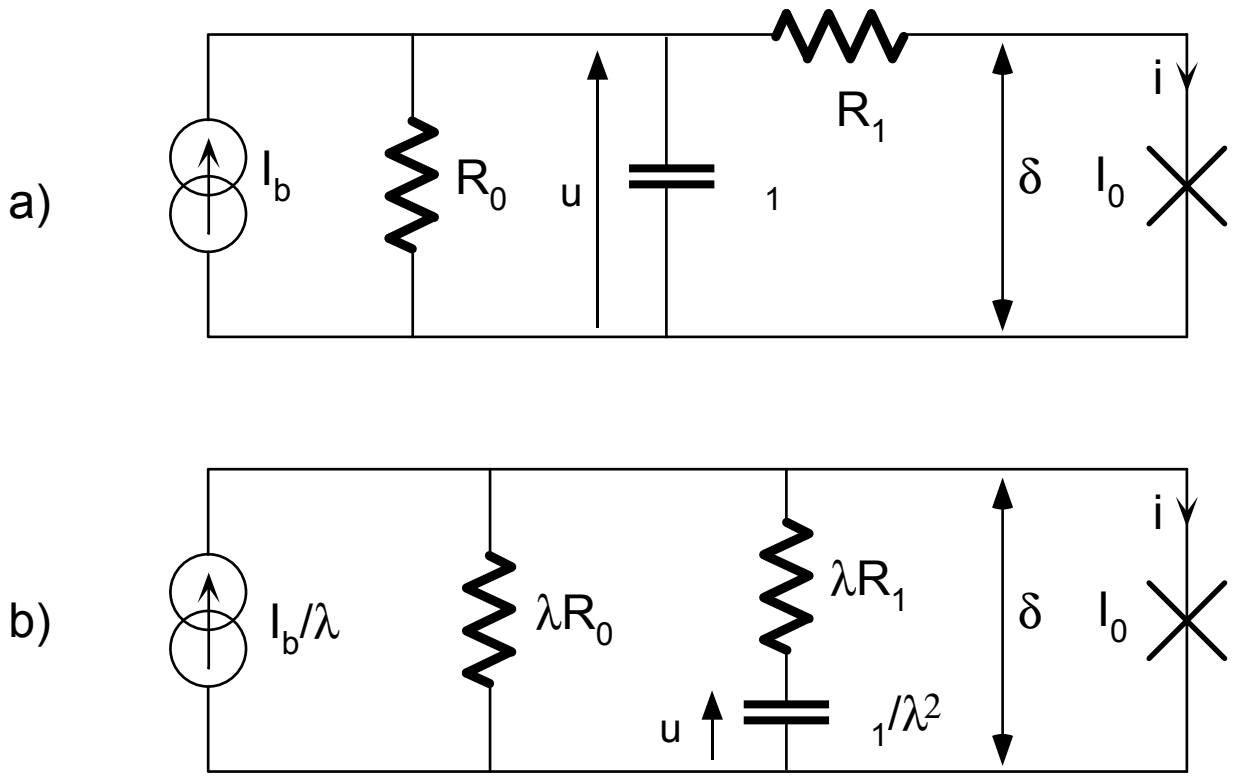
a)
$I_b$
$R_0$
u
1
$R_1$
δ
$I_0$
i
b)
$I_b/\lambda$
$\lambda R_0$
$\lambda R_1$
u
$_1/\lambda^2$
δ
$I_0$
i

Fig.

Fig. 5

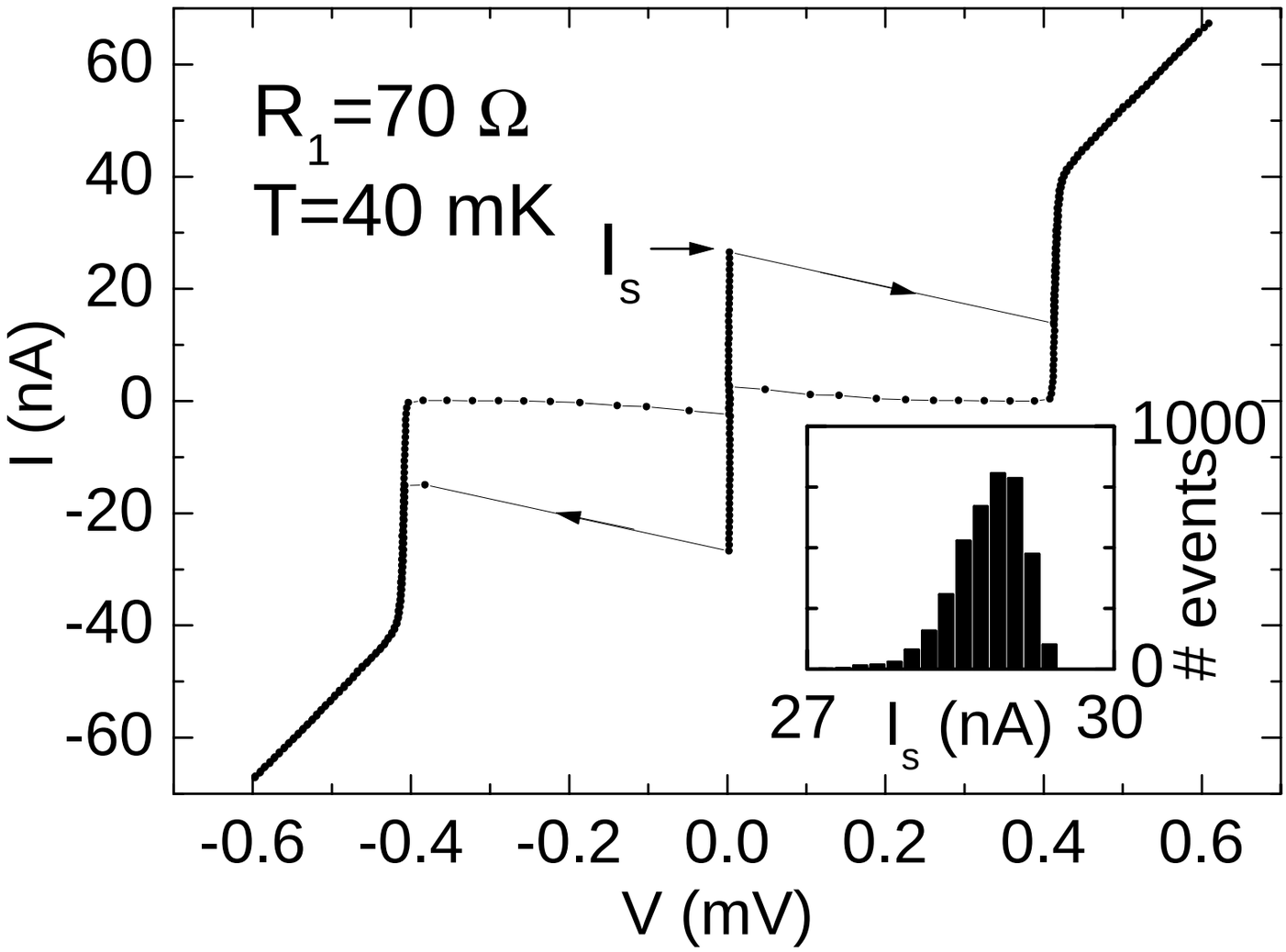
R1=70 Ω
T=40 mK
Is
I (nA)
V (mV)
60
40
20
0
-20
-40
-60
-0.6
-0.4
-0.2
0.0
0.2
0.4
0.6
1000
0
# events
27
Is (nA)
30

Fig. 6

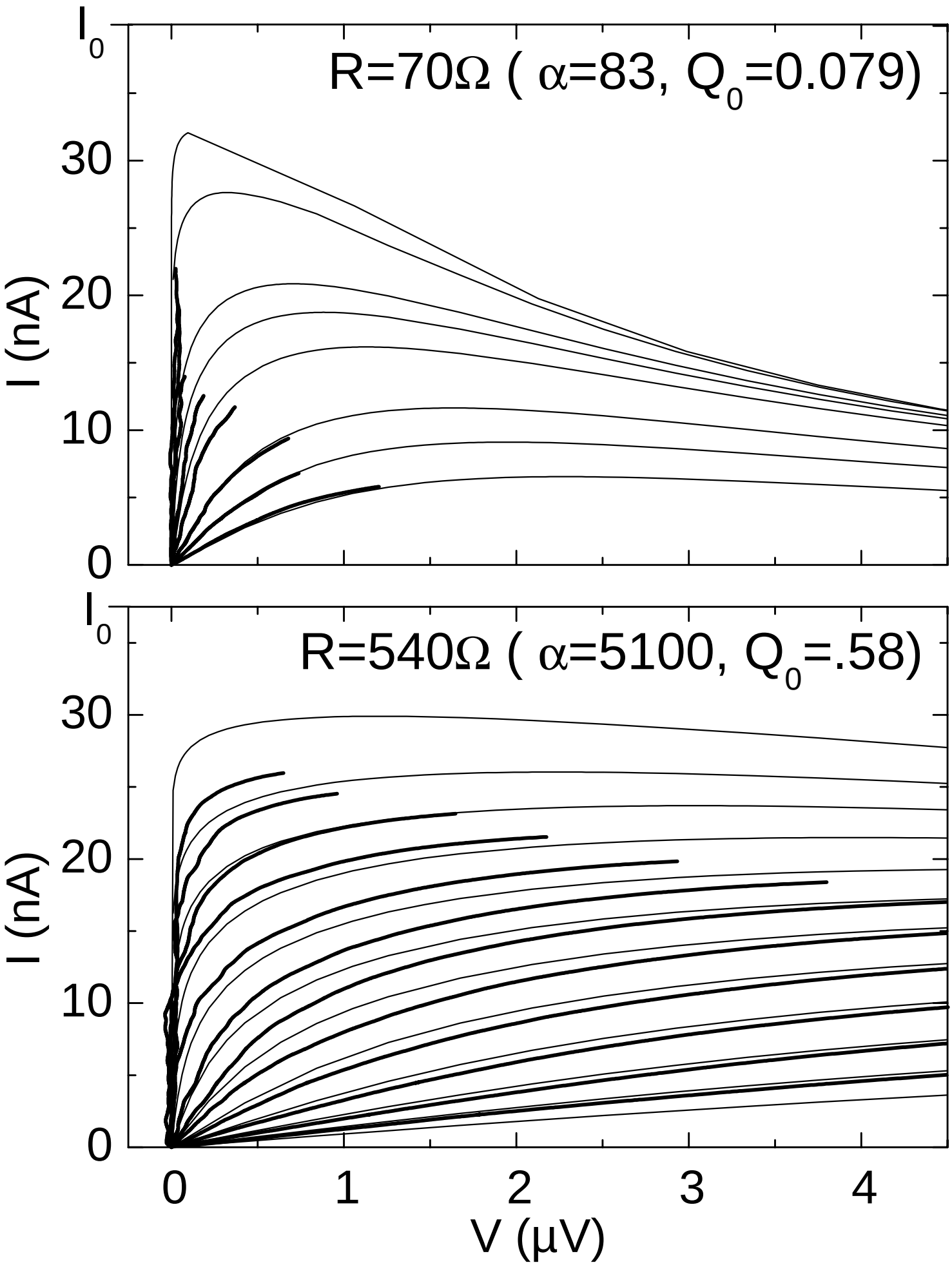
I0
R=70Ω ( α=83, Q0=0.079)
30
20
10
0
I (nA)
I0
R=540Ω ( α=5100, Q0=.58)
30
20
10
0
I (nA)
0
1
2
3
4
V (μV)

Fig. 7

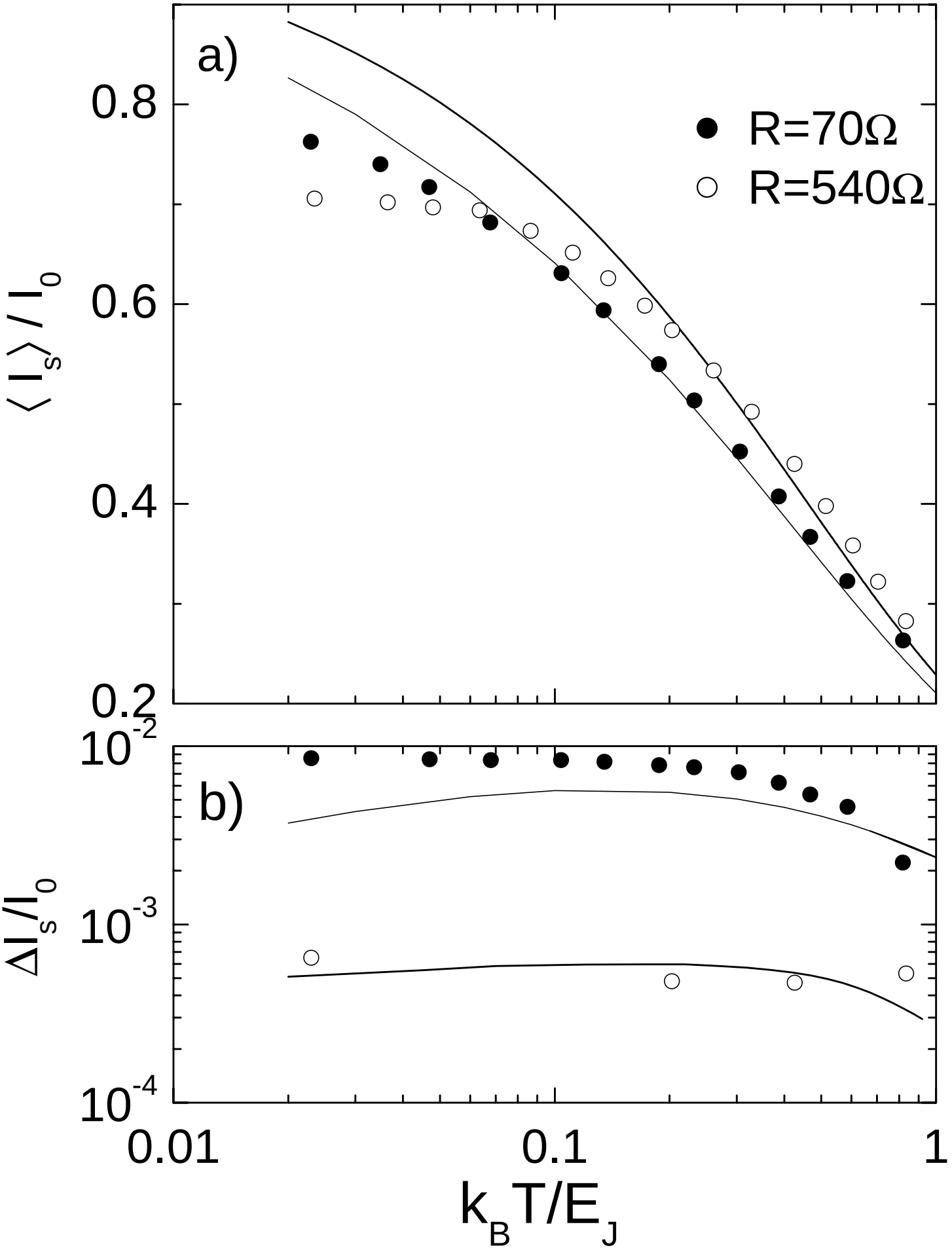
a)
b)
R=70Ω
R=540Ω
0.8
0.6
0.4
0.2
$\langle I_s \rangle / I_0$
$10^{-2}$
$10^{-3}$
$10^{-4}$
$\Delta I_s / I_0$
0.01
0.1
1
$k_B T/E_J$

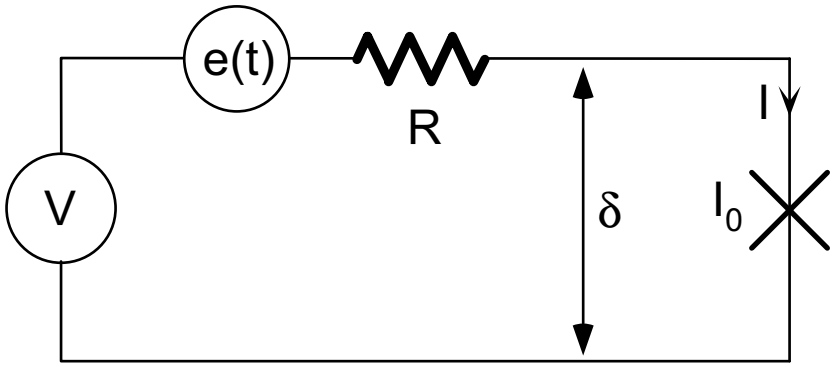


Fig. 8